Journal of Geoscience and Environment Protection, 2023, 11, 1-12
https://www.scirp.org/journal/gep
ISSN Online: 2327-4344
ISSN Print: 2327-4336

# Flood Vulnerability Assessment Using Satellite Imagery Data

**Efthymia Koliokosta**

Department of Shipping, Trade and Transport, University of the Aegean, Chios, Greece
Email: efigrx@yahoo.com

**How to cite this paper:** Koliokosta, E. (2023). Flood Vulnerability Assessment Using Satellite Imagery Data. *Journal of Geoscience and Environment Protection, 11,* 1-12.
https://doi.org/10.4236/gep.2023.1112001

**Received:** November 5, 2023
**Accepted:** December 5, 2023
**Published:** December 8, 2023



## Abstract

As flood extreme occurrences are projected to increase in intense and frequency due to climate change, the assessment of vulnerability and the identification of the most vulnerable areas, populations, assets and systems are an urgent need. Vulnerability has been widely discussed and several flood projection tools have been developed using complex hydrological models. However, despite the significant contribution of flood projection maps to predicting the impact of potential floods, they are difficult and impractical to use by stakeholders and policy makers, while they have proven to be inefficient and out of date in several cases. This research aims to cover the gaps in coastal and riverine flood management, developing a method that models flood patterns, using geospatial data of past large flood disasters. The outcomes of this research produce a five scale vulnerability assessment method, which could be widely implemented in all sectors, including transport, critical infrastructure, public health, tourism, constructions etc. Moreover, they could facilitate decision making and provide a wide range of implementation by all stakeholders, insurance agents, land-use planners, risk experts and of course individual. According to this research, the majority of the elements exposed to flood hazards, lay at specific combinations between 1) elevation (Ei) and 2) distance from water-masses (Di), expressed as (Ei, Di), including: 1) in general landscapes: ([0 m, 1 m), [0 km, 6 km), [0 m - 3 m), [0 km, 3 km)) and ([0 m - 6 m), [0 km, 1 km)), 2) in low laying regions: ([0 m, 1 m), [0 km, 40 km), [0 m - 3 m), [0 km, 30 km)) and ([0 m - 6 m), [0 km, 15 km)) and 2) in riverine regions: ([0 m, 4 m), [0 km, 3 km)). All elements laying on these elevations and distances from water masses are considered extremely and highly vulnerable to flood extremes.

## Keywords

Coastal Flood, Riverine Flood, Vulnerability Assessment, Retrospective Analysis, Policy Making, Decision Making, Sustainability

## 1. Introduction

Climate change has increased the frequency and intensity of climate extreme occurrences. Among them, large hydrological disasters due to coastal and riverine flooding demonstrate the highest damages and financial burden (Koliokosta, 2017; Woodruff et al., 2013). Vulnerability is a fuzzy concept encompassing variable definitions (Koliokosta, 2023) expressed by exposure, susceptibility and coping capacity (Taubenböck et al., 2008). However, due to gaps in susceptibility assessment methodologies that could be widely used for all types of elements (i.e. humans, critical infrastructure, cultural elements, industrial elements etc.) and the lack of information and knowledge in assessing the adaptive capacity and the efficiency of preventive measures (Nateghi et al., 2016; Piadeh et al., 2022), exposure is the dominant vulnerability factor (i.e. Koliokosta, 2022) when discussing coastal, riverine and estuarial areas (Voice et al., 2006; Bernhofen et al., 2021). Adaptative capacity is widely concerned as the flip side of vulnerability (Rose & Krausmann, 2013) and is strongly associated to the level of development and economic growth. However, in the case of flood extremes this myth is strongly debunked, as developed and high capacity countries perform high financial burden due to flood disasters (EM-DAT; Koliokosta, 2022). Thus, adaptative capacity should be very carefully and frugally used when assessing flood vulnerability.

Despite the plethora of flood mapping methods and tools (i.e. MIKEFLOOD, HEC-RAC, Arc-GIS, FlowRoute, FlowRouteTM, FloodFutures etc.), uncertainties, derived from lack of hydrological data, such as rainfall and runoff inputs, extreme value statistics of flooding events (Galambos et al., 1993) and modelling techniques (Zahmatkesh et al., 2021), still exist and need to be furtherly concerned. Flood simulations, as a tool, are rarely used by practitioners and decision makers in flood risk management, due to high complexity in implementation especially under emergency situations when rapid decisions under uncertainties need to be taken (Zhang et al., 2022). Moreover, flood simulations might also make inaccurate conclusions, inadequate to produce consistent information for effective flood disaster management (US GAO, 2021). Finally, there are significant inconsistencies between the outcomes of flood projection maps and the results of other climatic projection methods (i.e. Koriche et al., 2021; Ataei et al., 2018), which might complicate policy and decision making procedures.

The results of this research contribute to fill in the gaps in literature with respect to the existing uncertainties in flood projections. More specifically, this paper considers that data extracted from satellite images of previous large flooding events provide significant information about flood patterns, which define flood-water behavior and geospatial vulnerability (Antzoulatos et al., 2022). Satellite imagery could also reveal information about failures of preventive measures against hydrological hazards, which may lead to severe maladaptation (Fraser et al., 2012). Such information is crucial in decision making with respect to the identification and prioritization of adaptation needs and resilience investments.

## 2. Methods and Data

This research concerns 48 past riverine and coastal flood disasters (Table 1) and conducts a retrospective analysis of data extracted by satellite images provided by NASA Earth Observatory, Copernicus Emergency Service-Mapping-Sentinel Images, Maxar Satellite Imagery and NOAA Riverine Flood Inundation Maps. For the purposes of this research, satellite images are divided into congruent geographical strips, of approximately 100 m width, alongside the coastal and riverine inundated areas (Figure 1). Then, using Google Maps and GPS tools, random points on the maps are selected, developing a large database of 422.385 random points. These points are measured and assigned with metrics regarding: 1) the elevation Ei of a random point i relatively to sea or river level and 2) the distance Di of a point i to/from rivers and coastline. The analysis of these geospatial data, provide significant information, which has been used to define vulnerability zones and develop a vulnerability matrix, considering Ei and Di as the primary vulnerability factors for coastal hazard vulnerability ($V_C$) and riverine flood vulnerability ($V_R$,), concerning all types of landscapes, including general landscapes, low-laying regions, riverine and estuarial areas.

Table 1. Under-study coastal and fluvial inundation cases.

| Region | Description | Number of geographical points studied | |
|---|---|---|---|
| Australia, QND | Flinders River | 14.106 | https://earthobservatory.nasa.gov/images/144545/summer-floods-in-australia |
| Australia, QND | Leichhardt River | 11.598 | https://earthobservatory.nasa.gov/images/144545/summer-floods-in-australia |
| Australia, QND | Norman River | 11.543 | https://earthobservatory.nasa.gov/images/144545/summer-floods-in-australia |
| Australia, QND | Nicholson River | 13.303 | https://earthobservatory.nasa.gov/images/144545/summer-floods-in-australia |
| Australia, QND | Gregory River | 5.348 | https://earthobservatory.nasa.gov/images/144545/summer-floods-in-australia |
| Australia, QND-NSW | Brisbane River | 15.176 | https://earthobservatory.nasa.gov/images/48625/flooding-in-brisbane-suburbs |
| Australia, QND | Gilbert River | 3.521 | https://earthobservatory.nasa.gov/images/144545/summer-floods-in-australia |
| Australia, NSW-QND | Barwon and Gwydir Rivers | 4.132 | https://earthobservatory.nasa.gov/images/76677/flooding-in-australia |
| Australia, NSW | Hawkesbury River | 1.809 | https://www.abc.net.au/news/2021-03-27/satellite-images-show-flood-damage-in-windsor/100029758?utm_campaign=abc_news_web&utm_content=link&utm_medium=content_shared&utm_source=abc_news_web |
| Australia, NSW | Hastings River | 1.253 | https://emergency.copernicus.eu/mapping/system/files/components/EMSR504_AOI02_GRA_PRODUCT_r1_RTP01_v2.pdf |

**Continued**

| | | | |
|---|---|---|---|
| Brazil, Manaus | Negro River | 3.296 | https://earthobservatory.nasa.gov/images/39359/flooding-near-manaus-brazil |
| Vietnam and Cambodia | Mekong River | 1.9578 | https://earthobservatory.nasa.gov/images/17223/floods-in-cambodia |
| China (central) | Yangtze River and Dongting Hu LAke | 11.294 | https://earthobservatory.nasa.gov/images/18664/floods-in-central-china |
| China (central) | Li and Yuan Rivers | 8.385 | https://earthobservatory.nasa.gov/images/18664/floods-in-central-china |
| China (central) | Poyang Lake | 5.004 | https://earthobservatory.nasa.gov/images/146987/poyang-lake-extremes |
| India, Kerala | Kerala Rivers | 15.651 | https://earthobservatory.nasa.gov/images/92669/before-and-after-the-kerala-floods |
| India, Chennai | Adyar ElRiver | 8.062 | http://www.dmcii.com/wp-content/uploads/2016/03/Chennai_Map1.jpg |
| India, Tamil Nadu | Palar River | 12.038 | http://www.dmcii.com/wp-content/uploads/2016/03/Chennai_Map1.jpg |
| India, | Ganges Rives | 10.492 | https://earthobservatory.nasa.gov/images/73858/flooding-in-northern-india |
| India, Bihar | Koshi River | 8.581 | https://reliefweb.int/sites/reliefweb.int/files/resources/A3624A8177A5B215C12574B300442805-acted_FL_ind080824.pdf and https://earthobservatory.nasa.gov/images/9075/floods-cover-bihar-india |
| Myanmar, Irrawaddy Delta | Irrawaddy Delta | 12.394 | https://emergency.copernicus.eu/mapping/ems-product-component/EMSR130_16IRRAWADDYDELTA_DELINEATION_OVERVIEW-MONIT02/2 |
| Pakistan | Dasht River | 3.746 | https://earthobservatory.nasa.gov/images/146150/flash-flooding-in-iran |
| Iran, Hormozgan, Kerman, and Sistan-Baluchestan | Bahu Kalat River | 5.567 | https://earthobservatory.nasa.gov/images/146150/flash-flooding-in-iran |
| Romania, Galati | Danube River | 15.363 | https://www.esa.int/ESA_Multimedia/Images/2012/05/Danube_flood_mapping |
| Poland, Trześń | Vestula River | 12.947 | https://earthobservatory.nasa.gov/images/44102/vistula-river-flooding-southeastern-poland |
| Hungary, Vác | Danube River | 11.511 | https://earthobservatory.nasa.gov/images/2743/danube-river-flooding-near-vac-hungary |
| Hungary-Croatia | Danube River | 12.200 | https://earthobservatory.nasa.gov/images/9374/flooding-along-the-danube-river |
| Germany-Belgium-The Netherlands | Meuse and Roer Rivers | 7.688 | https://earthobservatory.nasa.gov/images/148598/deadly-floods-surprise-europe |
| Greece, Thessaly | Sofaditis River | 1.203 | https://rapidmapping.emergency.copernicus.eu/EMSR692/download |
| Greece, Thessaly | Kalentzis River | 1.020 | https://rapidmapping.emergency.copernicus.eu/EMSR692/download |
| Greece, Thessaly | Pinios Rivier | 2.105 | https://rapidmapping.emergency.copernicus.eu/EMSR692/download |
| Germany, Hitzacker | Elbe River | 5.126 | https://www.esa.int/Applications/Observing_the_Earth/Massive_German_floods_monitored_from_space |
| Germany, Wittenberg | Elbe River | 5.567 | https://earthobservatory.nasa.gov/images/2731/flooding-in-germany |

**Continued**

| | | | |
|---|---|---|---|
| Greece, Feres-Turkey | Evros River | 3.874 | https://emergency.copernicus.eu/mapping/ems-product-component/EMSR277_03FERES_01DELINEATION_MONIT01/1 |
| Greece, Didimoteiho-Turkey | Evros River | 2.568 | https://emergency.copernicus.eu/mapping/ems-product-component/EMSR277_02DIDIMOTICHO_01DELINEATION_MONIT01/2 |
| Dakota, Iowa, and Kansas | Mississippi, Illinois and Missouri Rivers | 8.849 | https://earthobservatory.nasa.gov/images/145029/flooding-continues-along-the-mississippi |
| Mississippi and Louisiana | Mississippi River | 13.753 | https://earthobservatory.nasa.gov/images/87305/flooding-on-the-lower-mississippi |
| Canada, Vancuver | Nooksack River | 7.350 | https://earthobservatory.nasa.gov/images/149100/severe-flooding-in-the-pacific-northwest538 |
| Bahamas Islands | Hurricane Dorian | 15.038 | https://earthobservatory.nasa.gov/images/145584/in-the-wake-of-hurricane-dorian |
| Texas, High Island | Hurricane Ike | 13.606 | https://earthobservatory.nasa.gov/images/9107/hurricane-ike-impact-on-high-island-texas |
| Louisiana, New Orleans | Hurricane Katrina | 19.834 | https://earthobservatory.nasa.gov/images/15419/hurricane-katrina-floods-the-southeastern-united-states |
| Louisiana and Texas, Houston | Hurricane Harvey | 15.667 | https://www.nesdis.noaa.gov/news/noaa-satellites-and-aircraft-monitor-catastrophic-floods-hurricanes-harvey-irma |
| Florida, Ozello | Hurricane Idalia | 1.011 | https://earthobservatory.nasa.gov/images/15419/hurricane-katrina-floods-the-southeastern-united-states |
| Florida, Everglades | Hurricane Irma | 8.226 | https://www.nesdis.noaa.gov/news/noaa-satellites-and-aircraft-monitor-catastrophic-floods-hurricanes-harvey-irma |
| Virginia, Virginia Beach | Hurricane Florence | 7.673 | https://emergency.copernicus.eu/mapping/ems-product-component/EMSR311_12VIRGINIABEACH_01DELINEATION_MAP/2 |
| Japan | Japan Tsunami | 12.101 | https://www.esa.int/About_Us/ESRIN/Mapping_Japan_s_changed_landscape_from_space https://www.nasa.gov/topics/earth/features/japanquake/ishinomaki-20110315.html |
| Indonesia, Lhoknga | Indian Ocean Tsunami | 6.354 | https://www.nasa.gov/vision/earth/lookingatearth/indonesia_quake.html |
| Sri Lanka, Kalutara | Indian Ocean Tsunami | 5.874 | https://www.nasa.gov/vision/earth/lookingatearth/indonesia_quake.html |

Sources: Authors' measurements

The database produced from the Ei and Di measurements of the selected geographical points, concerns 317.001 and 105.384 points for riverine and coastal flooding accordingly. A sample of the database is described at **Table 2**. The selected points lay exclusively within the limits of the flooded areas highlighting the flood edge-line, which actually outlines the limits of the flooded area (Koliokosta, 2022).


Source: https://earthobservatory.nasa.gov. Adapted to Author's adjustments.

**Figure 1.** Flooded areas division in zones and study of random geographical points.

**Table 2.** Sample of the geospatial database extracted from satellite image data.

| Geographical Points | Map Coordinates | Elevation | Distance from coastline | Distance from rivers |
|---|---|---|---|---|
| 1 | 30.026510846743175, −90.09126374367264 | 1 m | 0.3 km | 0.5 km |
| 2 | 30.021271734151462, −90.0876803125315 | 1 m | 0.7 km | 0.4 km |
| 3 | 30.01446233185223, −90.10851571205833 | 1 m | 1.5 km | 0.9 km |
| 4 | 30.00385091733764, −90.07886476979077 | 1 m | 2.7 km | 0.5 km |
| 5 | 29.966015017386045, −90.0665051847894 | 1 m | 7.2 km | 1.1 km |

## 3. Results

### 3.1. Coastal Flooding Vulnerability

In natural elevation regions, the majority of the geographical points (appr. 65%) lay low at elevations that do not exceed 1 m from the sea level, with almost 52% to lay within 3 km from the coastline, while almost half of them lay close to the coastline (<1 km) and elevations < 3 m (**Figure 2**). In low laying regions approximately 56% of the inundated points lay at elevations < 1 m from the sea level and distances < 30 km from the sea shore, while 55% of them are densely found within 15 km from the coastline and elevations < 3 m (**Figure 2**). In all cases, more than 50% of the total points lay on the above combination (Ei, Di), which construct the "extremely vulnerable" vulnerability zones (**Figure 2** and **Figure 4**).

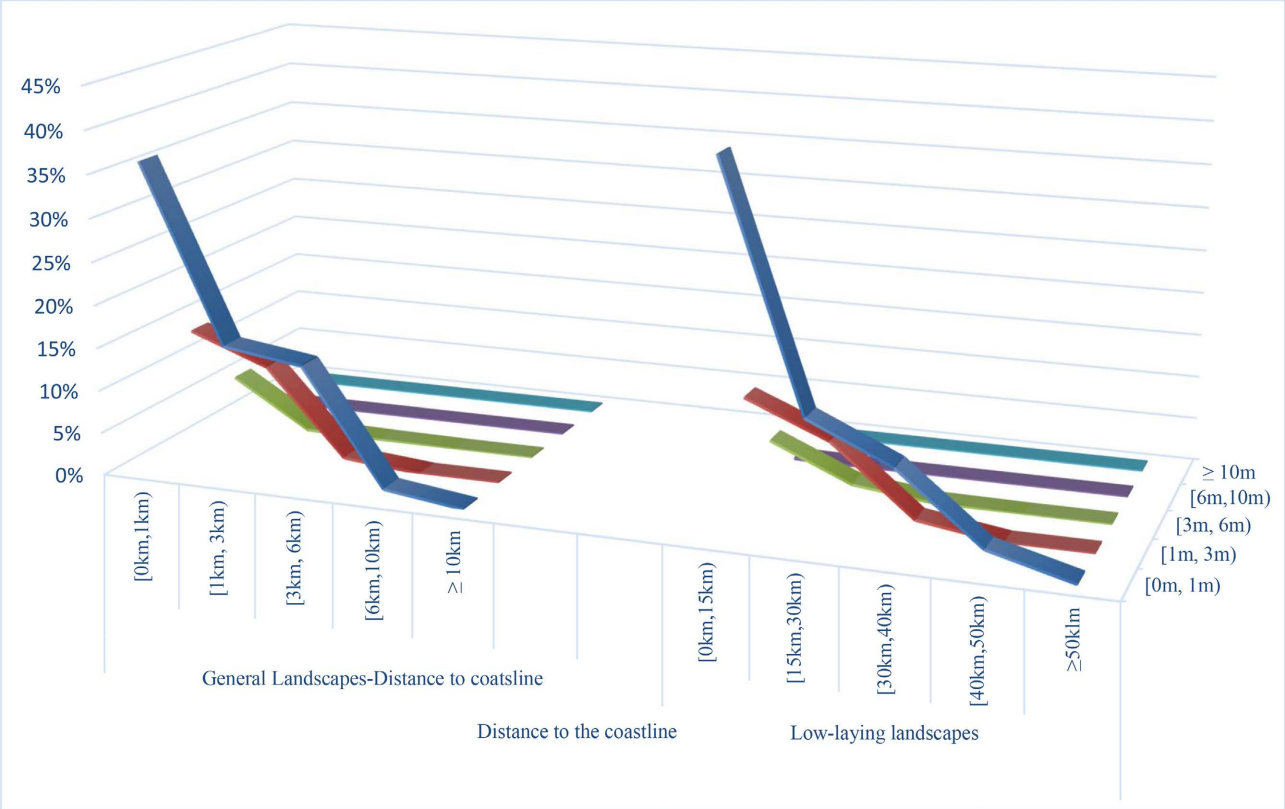


**Figure 2.** Geographical points' distribution by landscape, elevation and distance from water-masses.

Correspondingly, the statistical analysis of the geospatial points concludes that almost one third of the selected points in general landscapes lay at elevations < 6 m from the sea level, with the majority of them (appr. 14%) to lay at the low elevations (<1 m) and distances ranging between [3 km, 6 km) from the coastline (**Figure 2**). The remaining 17% of the flooded points lay at higher elevations and distances closer to the seashore, with only 6% of the points to lay on elevations between [3 m, 6 m) from the sea level and distances < 1 km from the coast line. In low elevation areas, almost 25% of flood waters penetrate inland for several km, as they transfer through other inland water-masses at elevations close to sea level, with 10% of the points to lay at a 30 km - 40 km distance from the sea shore. Even at higher elevations, [1 m, 3 m) and [3 m, 6 m), the according 9% and 5% of the selected points have faced severe inundation at farther distances ranging between [15 km, 30 km) and [30 km, 40 km) respectively (**Figure 2**). As these areas face also high exposure to coastal flooding they could be considered as "highly vulnerable" to flood extremes (**Figure 4**).

As Di and Ei increase, the frequency of flooded findings reduces dramatically. In general landscapes, only 2% of the selected points are exposed to coastal hazards in all Ei-Di combinations, with Ei $\in$ [3 m, 6 m) from the sea level and Dc $\in$ [6 mk, 10 km) from the coastline. In low laying regions, only 0.2% of the selected points are found at much higher elevations within [6 m, 10 m) from the sea level when the distance from the coastline does not exceed 15 km. The ma-

jority, approximately 3% of the selected points are concentrated at low elevations (≤1 m) and longer distances [40 km, 50 km) from the coastline. Despite the low frequencies in inundated points findings in these Ei-Di combinations, they are not negligible and thus they could constitute the "moderate vulnerability" zone for coastal hazards (**Figure 2** and **Figure 4**).

### 3.2. Riverine Flooding Vulnerability

In the case of riverine inundation, the distance from the river is the primary exposure factor that defines vulnerability and not elevation, as the later may perform high variability along its route. Moreover, as all elements laying at elevations higher than 4 m from the river elevation can be considered resilient to riverine flood (NOAA, 2018), the distance Di is the dominant vulnerability factor, which tends to be higher at the sharp "Us" of the rivers (Koliokosta, 2022).

According to the database analysis, almost 68% of the flooded points selected lay at distances < 1 km from the river edge, (**Figure 3**), which coincides with the average width of rivers' floodplain, which is approximately 1 km (Tockner & Stanford, 2002). These areas are extremely exposed to riverine flood hazards, especially when then lay at lower elevations (**Figure 4**). The 27% of the points laying at Di $\in$ [1 km, 3 km) face the highest exposure and thus they define the "extremely vulnerable" flood zone (**Figure 4**), which is very frequently flooded by the connected Creeks or smaller streams that enhance the inundation at more distant regions and may cause inundation deeper than 3 m. The remaining 4% of the points laying at Di $\in$ [3 km, 5 km) form the moderate vulnerability zone, where despite the smaller inundation impact, it needs to be furtherly concerned in land-use planning as they might face higher vulnerability in future due to more extreme precipitation occurrences.

Due to low atmospheric pressure-oriented climate extremes interconnection, coastal and estuarial regions are exposed to compound hazards, including extreme precipitation, storm surges, high winds and high tides (Zhang et al., 2018).

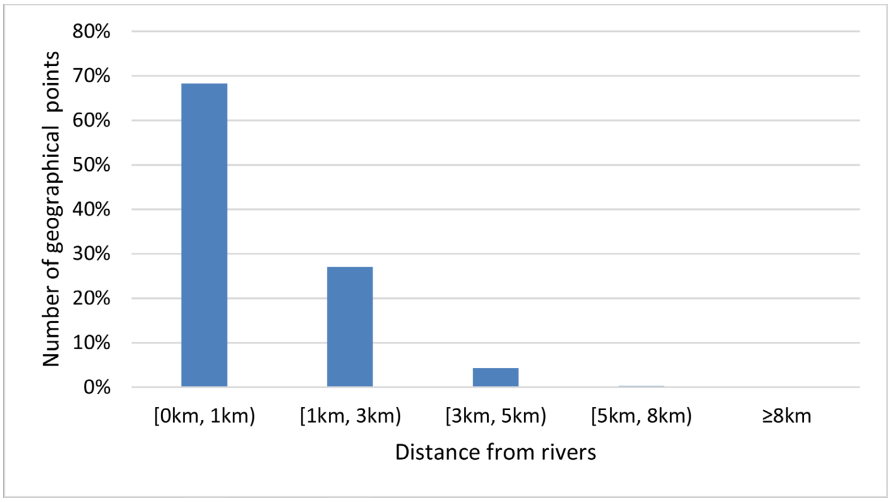


**Figure 3.** Distribution of the geographical points' distribution by distance.

| | | | *Distance to the coastline* | | | | | |
|---|---|---|---|---|---|---|---|---|
| Vulnerability to coastal hazards (Sea level rise, high tides and storm surges), $V_C$ | General landscapes (SLR and storm surges) $V_C$ | ***Elevation*** | **[0km,1km) 1** | **[1km, 3km) 2** | **[3km, 6km) 3** | **[6km,10km) 4** | **≥ 10km 5** | ***Scales*** |
| | | **[0m, 1m)** | Extreme | Extreme | High | Moderate | Low | **5** |
| | | **[1m, 3m)** | Extreme | High | Moderate | Low | Very low | **4** |
| | | **[3m, 6m)** | High | Moderate | Low | Low | Very low | **3** |
| | | **[6m,10m)** | Moderate | Low | Low | Very low | Very low | **2** |
| | | **≥ 10m** | Low | Very low | Very low | Very low | Very low | **1** |
| | | | ***Distance to the coastline*** | | | | | |
| | Low-laying landscapes (SLR and storm surges) $V_C$ | ***Elevation*** | **[0km,15km) 1** | **[15km,30km) 2** | **[30km,40km) 3** | **[40km,50km) 4** | **≥50klm 5** | **Scales** |
| | | **[0m, 1m)** | Extreme | Extreme | High | Moderate | Low | **5** |
| | | **[1m, 3m)** | Extreme | High | Moderate | Low | Very low | **4** |
| | | **[3m, 6m)** | High | Moderate | Low | Low | Very low | **3** |
| | | **[6m,10m)** | Moderate | Low | Low | Very low | Very low | **2** |
| | | **≥ 10m** | Low | Very low | Very low | Very low | Very low | **1** |
| | | | ***Distance from rivers*** | | | | | |
| Vulnerability to Riverine flooding due to extreme precipitation, $V_R$ | Riverine regions $V_R$ | Elevation ≤ 4m | [0km, 1km) **Extreme 5** | [1km, 3km) **High 4** | [3km, 5km) **Moderate 3** | [5km, 8km) **Low 2** | ≥8km **Very low 1** | |
| | Coastal and estuarial regions far from rivers $V_R$ | | Similar with $V_C$ | Similar with $V_C$ | Similar with $V_C$ | - | - | |

**Figure 4.** Flood vulnerability zones for coastal and riverine areas due to climate extremes.

Thus, in this case, coastal and estuarial areas, not connected to or distant from rivers and other water-masses, will be assigned with the higher level of coastal vulnerability ($V_C$) and not the negligible riverine inundation vulnerability ($V_R$), when concerning extreme precipitation vulnerability (**Figure 4**).

## 4. Discussion

The contribution of satellite images to flood vulnerability assessment and mapping is significant as they provide us with knowledge and information about flood-water behavior and patterns, which can be used for the development of vulnerability zones definition. This method could be used to assess the vulnerability of all types of elements, including exposed populations, transport infrastructure, critical infrastructure and other systems and networks. **Table 3** is indicative of the wide range of implementation of this method in vulnerability assessment in a [1, 5] scale, which can be also used in risk assessment (Koliokosta, 2023). According to **Table 3**, the suggested vulnerability assessment methodology can be applied on Airports, Highways, Rail Network, Hospitals, Museums and UNESCO Cultural Heritage Sites, Universities, Nuclear Plants in different places and landscapes around the world.

This method, also, could be useful in urgent and emergency situations that

Table 3. Vulnerability assessment.

| Element | Vulnerability to coastal hazards* | Riverine flood due to extreme precipitation vulnerability** |
|---|---|---|
| Sydney Kingsford Smith International Airport, Australia | 5 | 5 |
| Highway A1, Pacific Highway-Hexham 2322 NSW, Australia | 4 | 5 |
| Royal Prince Alfred Hospital | 1 | 1 |
| Sandalford Winery, Perth, Australia | 1 | 5 |
| Tokyo Rail Station, Tokyo, Japan | 1 | 1 |
| Shijō-mae Rail Station, Greater Tokyo, Japan | 5 | 5 |
| Aomi Station, Greater Tokyo, Japan | 5 | 5 |
| Fukushima Daiichi Nuclear Power Plant, Japan | 4 | 4 |
| Thessaloniki International Airport Macedonia, Greece | 5 | 5 |
| Ioannis Kapodistrias International Airport, Corfu, Greece | 5 | 5 |
| Kaohsiung International Airport, China | 4 | 5 |
| Medieval City of Rhodes, Greece ((UNESCO heritage site) | 1 | 1 |
| Chennai International Airport, Chennai, India | 2 | 5 |
| Hawaii University, Maui College, Hawaii, USA | 5 | 5 |
| Harvard University, Massachusetts, Cambridge, USA | 5 | 5 |
| Ritz Carlton Hotel, Los Angeles, California, USA | 5 | 5 |
| Alaska Native Medical Center, Anchorage, Alaska, USA | 1 | 5 |
| Samuel Simmonds Memorial Hospital, Utqiaġvik, Alaska, USA | 2 | 5 |
| Pomorski muzej, Dubrovnik Old Town, Croatia (UNESCO heritage site) | 3 | 3 |

*Refers to all coastal elements; **Refers to all riverine elements as wells as coastal and estuarial elements distant from rivers.

need rapid decision making, when complex hydrological model or other flood projection techniques cannot timely provide. Finally, the suggested vulnerability matrix could be combined with other flood projection tools in order to increase the accuracy of the flood projection outcomes and provide accurate vulnerability information in decision and policy making, land-use planning and risk assessment in all sectors, including critical infrastructure, public health, tourism, national defense, culture etc.

## 5. Conclusion

This research suggests a methodology for assessing coastal and riverine flooding due to climate extremes, using geospatial data exported from satellite imageries. The suggested method considers that past flood disasters provide significant information about flood patterns and flood-water behavior in regions with different geomorphology and geographical features, which can be used to model coastal and riverine vulnerability. A retrospective analysis of past large

floods has concluded to the development of vulnerability matrices, based on elevation and distance from water-masses, based on the frequency of the findings within specific Ei-Di combinations in the flooded areas.

The advantage of this vulnerability assessment method relatively to complex hydrological models, is that it is very easy to understand and use by all decision makers and stakeholders around the world. This could facilitate decision making with respect to the identification and prioritization of adaptation and resilience investments against flood disasters. This could be time and cost effective, as vulnerability assessment can be done using only GPS data, which are accessible to everyone. Moreover, this method has a wide range of implementation on all sectors, including critical infrastructure, hospitality and cultural risk management, nuclear plants planning and safety, national defense, health care system and public health, educational institutes planning and management, agriculture and wineries, etc. Finally, the outcomes of this method could be concerned parallel with other flood projection tools in order to optimize their efficiency and the accuracy of flood risk management.

## Conflicts of Interest

The author declares no conflicts of interest regarding the publication of this paper.

## References

Antzoulatos, G., Kouloglou, I., Bakratsas, M., Moumtzidou, A., Gialampoukidis, I., Karakostas, A., Lombardo, F., Fiorin, R., Norbiato, D., Ferri, M. et al. (2022). Flood Hazard and Risk Mapping by Applying an Explainable Machine Learning Framework Using Satellite Imagery and GIS Data. *Sustainability, 14,* Article 3251. https://doi.org/10.3390/su14063251

Ataei, H. S., Jabari, Kh. A., Khakpour, A. M., Adjami, M., & Neshaei, S. A. (2018). Investigation of Caspian Sea Level Fluctuations Based on ECMWF Satellite Imaging Models and Rivers Discharge. *International Journal of Coastal & Offshore Engineering, 2,* 21-30. https://doi.org/10.29252/ijcoe.2.2.21

Bernhofen, M. V., Trigg, M. A., Sleigh, P. A., Sampson, C. C., & Smith, A. M. (2021). Global Flood Exposure from Different Sized Rivers. *Natural Hazards and Earth System Sciences, 21,* 2829-2847. https://doi.org/10.5194/nhess-21-2829-2021

*Emergency Events Data Base EM-DAT.* https://www.emdat.be

Fraser, S., Raby, A., Pomonis, A., Goda, K., Chian, S. C., Macabuag, J., Offord, M., Saito, K., & Sammonds, P. (2012). Tsunami Damage to Coastal Defences and Buildings in the March 11th 2011 $M_w$ 9.0 Great East Japan Earthquake and Tsunami. *Bulletin of Earthquake Engineering, 11,* 205-239. https://doi.org/10.1007/s10518-012-9348-9

Galambos, J., Lechner, J., Simiu, E., & Hagwood, C. (1993). *Extreme Value Theory and Applications. Proceedings of the Conference on Extreme Value Theory and Applications, Volume 3* (p. 231). NIST Special Publication 860, Springer.

Koliokosta, E. (2017). Publications of Climate Change Impact on Transport Infrastructure. In *96th Annual Meeting of the Transportation Research Board.*

Koliokosta, E. (2022). Geospatial Assessment of Transport Infrastructure Vulnerability to Flooding Events. In *Proceedings of the International Conference on Natural Hazards and Infrastructure, International 3rd Conference on Natural Hazards and Infrastruc-*

*ture.*

Koliokosta, E. (2023). Impact Assessment of Climate Change on Public Health: A Global Perspective. *Environmental Sciences Proceedings, 26,* Article 68. https://doi.org/10.3390/environsciproc2023026068

Koriche, S., Singarayer, J., & Cloke, H. (2021). The Fate of the Caspian Sea under Projected Climate Change and Water Extraction during the 21st Century. *Environmental Research Letters, 16,* Article 094024. https://doi.org/10.1088/1748-9326/ac1af5

Nateghi, R., Bricker, J. D., Guikema, S. D., & Bessho, A. (2016). Statistical Analysis of the Effectiveness of Seawalls and Coastal Forests in Mitigating Tsunami Impacts in Iwate and Miyagi Prefectures. *PLOS ONE, 11,* e0158375. https://doi.org/10.1371/journal.pone.0158375

NOAA (2018). *North American Climate Extremes Monitoring.* https://www.ncei.noaa.gov/access/monitoring/cei/

Piadeh, F., Behzadian, K., & Alani, A. M. (2022). A Critical Review of Real-Time Modelling of Flood Forecasting in Urban Drainage Systems. *Journal of Hydrology, 607,* Article 127476. https://doi.org/10.1016/j.jhydrol.2022.127476

Rose, A., & Krausmann, E. (2013). An Economic Framework for the Development of a Resilience Index for Business Recovery. *International Journal of Disaster Risk Reduction, 5,* 73-83. https://doi.org/10.1016/j.ijdrr.2013.08.003

Taubenböck, H., Post, J., Roth, A., Zosseder, K., Strunz, G., & Dech, S. (2008). A Conceptual Vulnerability and Risk Framework as Outline to Identify Capabilities of Remote Sensing. *Natural Hazards and Earth System Sciences, 8,* 409-420. https://doi.org/10.5194/nhess-8-409-2008

Tockner, K., & Stanford, J. A. (2002). Riverine Flood Plains: Present State and Future Trends. *Environmental Conservation, 29,* 308-330. https://doi.org/10.1017/S037689290200022X

US GAO (2021). *United States Government Accountability Office (GAO) Report to Congressional Committees GAO-22-104079 (2021) FEMA 342 Flood Maps, Better Planning and Analysis Needed to Address Current and Future Flood Hazards* (p. 97). https://www.gao.gov/products/gao-22-104079

Voice, M., Harvey, N., & Walsh, K. (2006). *Vulnerability to Climate Change of Australia's Coastal Zone: Analysis of Gaps in Methods, Data and System Thresholds.* Report to the Australian Greenhouse Office.

Woodruff, J., Irish, J. L., & Camargo, J. (2013). Coastal Flooding by Tropical Cyclones and Sea-Level Rise. *Nature, 504,* 44-52. https://doi.org/10.1038/nature12855

Zahmatkesh, Z., Han, S., & Coulibaly, P. (2021). Understanding Uncertainty in Probabilistic Floodplain Mapping in the Time of Climate Change. *Water, 13,* Article 1248. https://doi.org/10.3390/w13091248

Zhang, K., Shalehy, Md. H., Ezaz, G. T., Chakraborty, A., Mohib, K. M., & Liu, L. (2022). An Integrated Flood Risk Assessment Approach Based on Coupled Hydrological-Hydraulic Modeling and Bottom-Up Hazard Vulnerability Analysis. *Environmental Modelling & Software, 148,* Article 105279. https://doi.org/10.1016/j.envsoft.2021.105279

Zhang, Q., Gu, X., Li, J., Shi, P., & Singh, V. P. (2018). The Impact of Tropical Cyclones on Extreme Precipitation over Coastal and Inland Areas of China and Its Association to ENSO. *Journal of Climate, 31,* 1865-1880. https://doi.org/10.1175/JCLI-D-17-0474.1